Technology and Health Care 12 (2004) 155–167
IOS Press

II. Biomaterials

Investigations of dynamic strength properties of plastics

C.A. Atroshenko[a], S.I. Krivosheev[b], Yu.V. Petrov[b], A.A. Utkin[b], G.D. Fedorovsky[b] and A.Yu. Petrov[b]
[a]*Institute for Problems of Mechanical Engineering RAS, St. Petersburg, Russia*
Tel.: 812 2475147; Fax: 812 3214771; E-mail: satroshe@atr.ipme.ru
[b]*St. Petersburg State University, St. Petersburg, Russia*

Introduction: It is well known, plastics and composites are widely used in medical fields. They may be capable of fulfilling functional requirement, relating not only to mechanical reliability but also to chemical one. Therefore it is important to know peculiarities of fracture mechanics of these materials.

Crack propagation is investigated experimentally in polymethylmethacrylate (PMMA) and glass microballoons filled composite material (GMFCM) under shock loading created impulse magnetic field. Microstructure features of dynamic fracture was analyzed.

Methods: Crack propagation is investigated experimentally in PMMA under shock loading created impulse magnetic field [3]. Loading scheme provided uniformly spread pressure along the crack banks. Plain specimens of PMMA 10 mm thick had notch 3 mm width and 10 cm length. Speed photo camera SFR-2 was used as photo register. Pressure amplitude constituted $P = 140$–320 MPa.

An experimental study of static and dynamic crack resistance of glass microballoons filled composite materials (GMFCM) that has a matrix of polyester resin containing a stuff of glass microspheres was conducted. The static mechanic characteristics of the material are established on the basis of data obtained by a standard static testing machine P-0.5 under tension velocity $1.67 \cdot 10^{-4}$ m/s [2]. Material contains 41% of glass microballoons by volume. In different samples the size of spheres was varied in intervals from 6–60 microns and also from 12–60 microns with average diameters from 21–31 microns. The density of the GMFCM, defined on weighing results was $\rho = 0.79 \pm 0.01 \times 10^3$ kg/m^3.

Results: An investigation has been made on PMMA with following mechanical properties: $c_1 = 1970$ m/s, $c_2 = 1130$ m/s, 1.47 MPam$^{1/2}$, where c_1 and c_2 are longitudinal and transverse wave elastic velocities, respectively, and K_{1c} is the critical stress intensity factor (static fracture toughness). The Young modulus under tension received from a standard test is $E = 2400 \pm 50$ MPa. The strength turned out to be equal $\sigma_c = 12.4 \pm 0.9$ MPa. The critical stress intensity factor (static fracture toughness) received from static tension tests on specimens containing central cracks is $K_{1c} = 0.52 \pm 0.03$ MPa$\sqrt{m}$. The longitudinal wave velocity, defined by interferometric method is $c_1 = 2196 \pm 50$ m/s. Propagating from the notch tip fracture character of PMMA changes from fiber, quasi-fiber to cup fracture like fracture types in metals. Diagram of different kinds of fracture depending on impulse duration and distance from notch tip is presented in [1]. This dependence has periodical character under loading of microsecond duration impulses of threshold amplitude. An illustration of the differences in fracture behavior and typical kinds of fracture character with their location along the main crack is given in [1]. Fracture character changing can be clearly seen.

The fracture energy, or the energy needed to create a unit fracture surfaces, is of tremendous practical and fundamental importance. For this reason, evaluation of the fracture energy as a function of the

crack velocity has been done. Surface fracture energy was evaluated, using cup size and specific surface fracture energy. Its dependence on distance from notch tip was defined [1].

The formation and evolution of meso-branches are a major influence of the dynamics of a crack. The existence of mesocracks that branch away from the main crack was discovered only in the places with fiber and quasi-fiber fracture types [1]. They did not find in the places of cup fracture. Inspection of the fracture surface in a given experiment shows that mesocrack inclination angle changes nonmonotonously depending on the distance from notch tip. Mesocrack inclination angles and places of their nucleation were determined. As for crack velocity, it has nonmonotonous character depending on distance from notch tip.

Fracture of glass microballoons filled composite materials mainly took place between glass spheres. Crack propagated along the binder rounding microballoons. Only in separate cases did it cross sphere. From the results of fractographical investigations of glass microballoons filled composite materials is clearly seen that the smaller filler grain size is the smaller final crack length [2]. It can be explained in such a manner: a longer quantity of glass spheres creates more barriers for crack movement.

From more detailed microstructure investigation under higher magnification we see the traces of irreversible deformation in binder and microcracks in some places around glass spheres. Under more magnification full details of binder fracture one can see characteristic peculiarities analogous to other polymers, such as polymethylmethacrylate, it has features of mirror, mist and hackle zones. The comparison of fracture character for static and dynamic loaded material could discover essentially more quantity of destroyed microballoons at the surface of static deformed materials, than under impulse loading.

The specific interphase surface between crack and matrix was determined using the method of quantitative metallography to define specific quantity of cracks branched from the main one for different samples and loads. It is clearly seen from data that these values in transverse directions are higher than in longitudinal one. It means that energy consumption for crack propagation is higher in transverse direction.

Conclusions: Peculiarities of fracture process are experimentally defined for polymethylmethacrylate (PMMA) and glass microballoons filled composite material (GMFCM) under shock loading on microsecond pulse duration of threshold amplitude.

References

[1] S.A. Atroshenko, S.I. Krivosheev and A.Yu. Petrov, Crack propagation upon dynamic failure of polymethylmethacrylate, *Technical Physics* **2** (2002), 194–199.

[2] S.A. Atroshenko, S.I. Krivosheev, Yu.V. Petrov, A.A. Utkin and G.D. Fedorovsky, Glass microballoons filled composite material fracture under static and dynamic loads, *Technical Physics* **12** (2002), 54–58.

[3] S.I. Krivosheev and Y.V. Petrov, Experimental Unit and the Method of Investigation of Threshold Fracture Loads for Macrocracked Samples under Impact Loading Produced by Pulse Magnetic Field, St.-Petersburg, 1997.

Response of Ti-Ni shape memory alloys to shock loading

C.A. Atroshenko[a], M.R. Edwards[b] and J.D. Painter[b]
[a]*Institute for Problems of Mechanical Engineering RAS, St. Petersburg, Russia*
Tel.: 812 2475147; Fax: 812 3214771; E-mail: satroshe@atr.ipme.ru
[b]*Cranfield University, Royal Military College of Science, Shrivenham, Swindon, UK*

Introduction: Since their biochemical stability is such an important factor when Shape Memory Alloys (SMA) are applied in medical field, almost all applications are limited to TiNi, despite the variety of SMAs available. Medical applications of TiNi include: orthopedics; dentistry; components in medical devices and instruments.

This material combines shape memory and superelastic properties. Therefore, it is important to know the behavior of this material under shock loading.

Methods: Materials under investigation were shape memory TiNi compositions containing 55.1% Ni and 47% Ni+3% Cu. The material was in the form of disk 15 mm in diameter or bar (□-23×18 mm) and their thickness varied from 1.6 to 4.5 mm. The explosive facility launched aluminum impactor plates 0.2 to 2.0 mm in thickness at velocities 600–700 m/s [2]. In the experiments, the free-surface velocity profiles were recorded with a Visar-type instrument. Microstucture investigations were carried out using SEM JEOL JSM 840 A. Microhardness was measured with the help HWDM-7.

Result: The results are presented in Table 1.

Using free surface velocity profile it was defined spall velocity (strength) for all investigated specimens. Results on spall strength are presented in Table 2.

From these data it is clearly seen Ti-Ni-Cu3 material has a higher spall strength than Ti-Ni. The highest spall strength ($W = 230 - 268$ m/s) occurred in Ti-Ni-Cu3 specimens shocked under loading velocity $V = 600 - -630$ m/s. Exactly these specimens have steps at the front part of the free surface velocity profiles before elastic precursor. Steps, induced proper transformation appear on this smooth part of compression wave. It means that martensite transformation takes place in these specimens during shock loading [1].

Table 1
Data on explosive experiments

No.	Material	Specimen size, mm	Al impactor thickness, mm	Flyer velocity, m/s
1	Ti-Ni-Cu3	□-23 × 18 × 4.5	2.0	700
2	Ti-Ni-Cu3	□-23 × 18 × 1.6	0.2	600
3	Ti44.9-Ni55.1	Ø-15 × 1.61	0.2	600
4	Ti-Ni-Cu3	□-23 × 18 × 4.42	2.0	700
5	Ti-Ni-Cu3	□-23 × 18 × 3.96	0.4	630
6	Ti-Ni-Cu3	□-23 × 18 × 4.47	0.4	630

Table 2
Spall strength

No.	W, m/s	V, m/s	Material	Specimen size, mm
1	100	700	Ti-Ni-Cu3	4.5 × 23 × 18
2	268	600	Ti-Ni-Cu3	1.6 × 23 × 18
3	94	600	Ti-Ni	1.61Ø15
4	180	700	Ti-Ni-Cu3	4.42 × 23 × 18
5	230	630	Ti-Ni-Cu3	3.96 × 23 × 18

Table 3
Microhardness of Ti-NiCu3 alloy

Condition	Microhardness, HV
Unshocked	203
After shock (V =630 m/s)	212

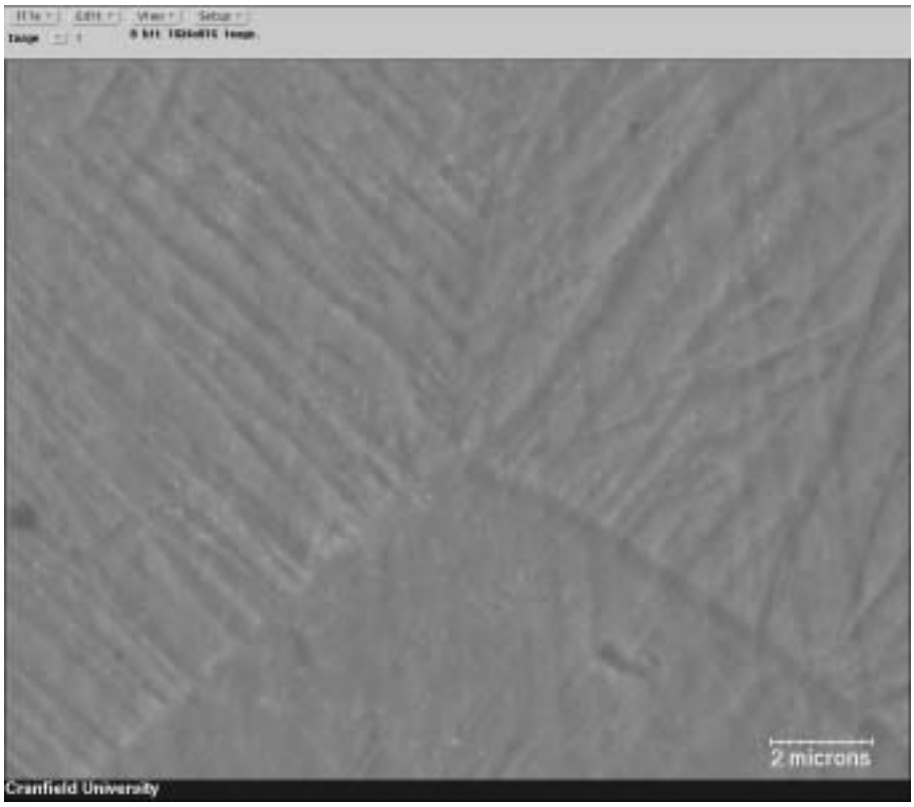

Fig. 1. Different orientations twinned martensite.

Microscopic examination of Ti-Ni-Cu3 specimen recovered from the shock with loading velocity 630 m/s revealed twinned martensite. This is clearly seen in Fig. 1.

Table 3 shows that the microhardness increased with shock wave loading.

The microhardness increased at velocity 630 m/s over the value measured for the unshocked alloy. It is connected with a phase change.

Conclusions: Compositions on the base of Ti-Ni shape memory alloy was investigated experimentally under shock loading in spall conditions. Spall strength turned out higher in Ti-Ni-Cu3 composition in comparison with Ti-Ni one. Microhardness increasing after shock loading under 630 m/s is connected with phase transformation. Exactly in this velocity range 600–630 m/s maximum of spall strength takes place.

Acknowledgment: Authors acknowledge colleagues from Institute for Problems of Chemical Physics RAS for explosive testing and useful discussions.

References

[1] S.A. Atroshenko and Yu.I. Mescheryakov, Propagation velocities of the fronts of martensitic transformations under impact loading of steels, *The Physics of Metals and Metallography* **3** (1997), 270–276.
[2] G.I. Kanel, S.V. Rasorenov, A.V. Utkin and V.E. Fortov, *Shock-wave phenomena in condensed matter*, Janus-K, Moscow, 1996.

Tissue engineered composite grafts (cartilage, keratinocytes, mucosa) for head and neck surgery

A. Haisch, M. Bücheler, M. Hanel, C. Schmidt, A. Schütz, S. Jovanovic and M. Sittinger
University Medical Center, Charite Campus Benjamin Franklin, Department of Otorhinolaryngology / HNO, Hindenburgdamm 30, 12200 Berlin, Germany
Tel.: +49 30 8445 2440; Fax: +49 30 8445 4460; E-mail: andreas.haisch@ukbf.fu-berlin.de; http://www.medizin.fu-berlin.de/hno/

Introduction: The topic of the investigation focuses on the combined *in vitro* and *in vivo* cultivation of human nasal chondrocytes, human nasal respiratory epithelium or human keratinocytes to provide composite grafts for head and neck surgery.

Methods: First, human nasal cartilage was harvested from nasal septal biopsies. Chondrocytes were encymatically isolated and amplified by monolayer culture. After 2 passages the chondrocytes were diluted within a solution of fibrinogen and injected into a PGLA-PGA fleece of $1 \times 1 \times 0.3$ cm of size. To finish the fixation of the chondrocytes, fibrin polymerization was induced by addition of thrombin. These constructs were subcutaneously implanted on the back of nude mice for 6–8 weeks.

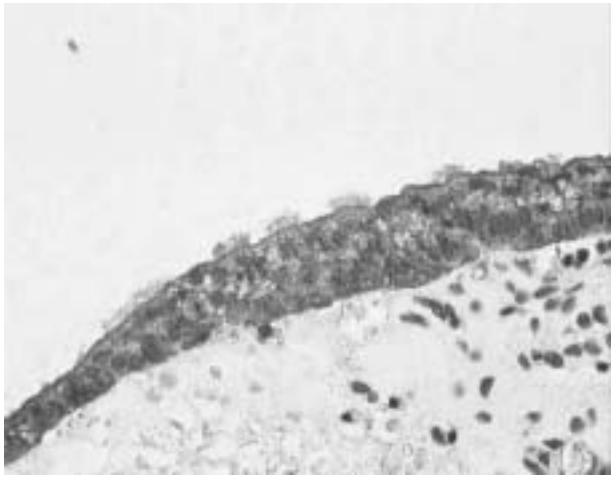

Fig. 1. Mucosa-cartilage contact zone, pancytoceratin immunostaining, $\times 40$.

Results: After this period, histochemical investigation showed neocartilage formation. Cartilage explants were incubated within a nutrition chamber and an explant culture of nasal mucosa was attached to the cartilage. Microscopic investigation of the composite grafts showed circumferent growth of a single layer of nasal ciliated epithelium on the cartilage explant up to 4 weeks (Fig. 1). The cartilage

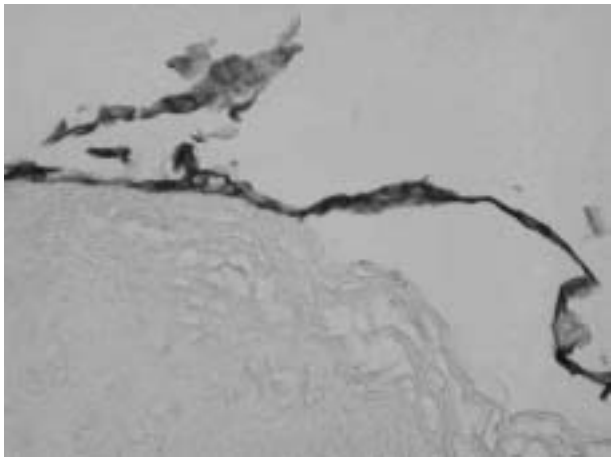

Fig. 2. Keratinocyte-sheet-cartilage contact zone, MNF immunostaining, $\times 20$.

showed a typical cartilage-like morphology during the entire period. In a second step, 1. isolated human keratinocytes, 2. keratinocyte sheets and 3. keratinocyte-fibrin suspension were seeded on the tissue engineered cartilage explants up to 4 weeks within an 'insert-culture' model. The 'insert culture' model allowes a biphasic nutritients supply to the tissue. The single cell keratinocyte culture and the keratinocyte-fibrin suspension cultures showed no attachment of the cells to the cartilage graft. The keratinocyte sheets demonstrated dissiminated attachment zones to the cartilage and a regular keratinocyte and cartilage morphology up to 4 weeks (Fig. 2). For tissue characterisation HE, Alcian, Vimentin, Cytokeratin und MNF staining was performed.

Summary: The investigations demonstrated first steps toward tissue engineered composite grafts for head and neck surgery. Based on these initial results explant culture for nasal mucosa-cartilage grafts and keratinocyte-fibrin insert culture for epidermal cartilage grafts could be favored for further investigations.

Composite stems of hip replacements with the gradient of elastic properties (GAP)

M. Petrtyl, A. Jïra and J. Danesova
Czech Technical University, Faculty of Civil Engineering, Laboratory of Biomechanics and Biomaterial Engineering, Prague, Czech Republic
Tel: +42 0224354479; Fax: +42 0224310775; E-mail: petrtyl@fsv.cvut.cz, ales.jira@fsv.cvut.cz

Introduction: The rigid metallic artificial replacements (implant stems) up-to-now applied in the clinical practice are classified as the artificial **replacements of the 1st generation**. Their substantial shortcomings include the limited possibilities of regulating the material properties. It is the composite polymer materials that make it possible to actively direct (influence) the properties of materials of a non-biological origin, as, for example, the magnitude of moduli of elasticity in compression, moduli of elasticity in tension, strength of materials etc. The composite stems of implants whose material properties will be very similar to those of a bone tissue are included in the group of artificial replacements of the 2nd generation.

The artificial replacements of the 2nd generation *are such implants that have very similar material/biometerial properties to the properties of a live tissue. These materials are biologically tolerated by*

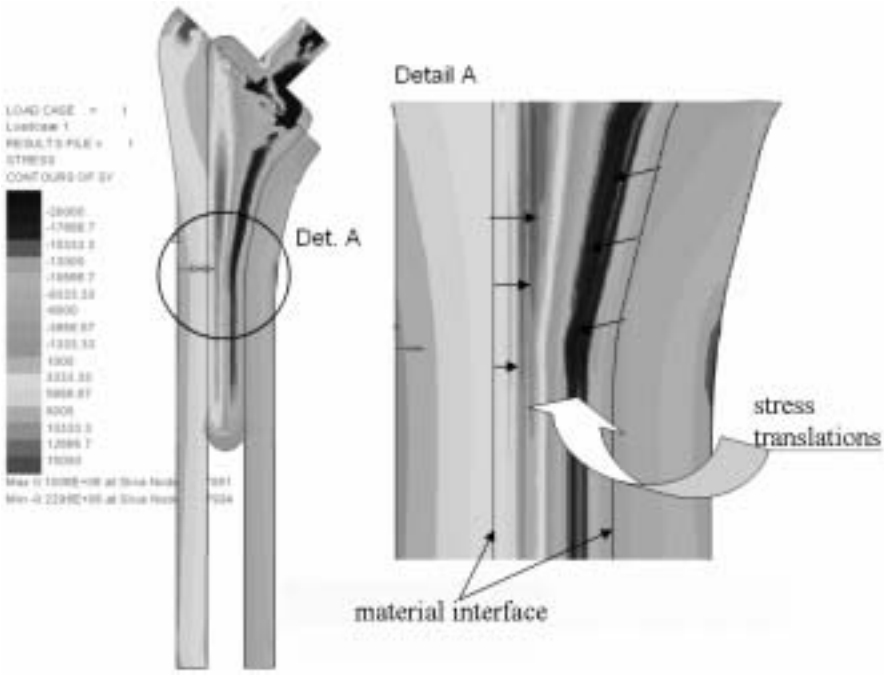

Fig. 1. Distributions of stress fields σ_y of the femur *diaphysis* – composite implant of the 2nd generation system (left); and detail A – increase in the stress fields σ_y.

a surrounding live tissue. After special treatment of stem surfaces, these materials create (*or support*) *the initiation of strong physical bonds with molecules of a connective tissue.*

The conditions of developing the physical bond interface of two completely different materials, ie a heterogeneous material (of a "visiting", non-biological origin) and a biological material, are strongly encouraged by identical deformations of the surface fibres of an inanimate implant and the fibres of a connective tissue. While the moduli of elasticity of the present-day rigid (metallic) implant stems of long bones, for example, are approximately ten times higher than those of the *corticalis* of *diaphyses*, in surface lamellas (composite stem laminas), a material with similar (or almost identical) material properties to those of the *corticalis* can be applied, i.e. $E = 18 - 20$ GPa.

Methods: Taking into account the high carrying capacity of artificial implant stems and their long-term stability in the femur *diaphyses*, the researchers have designed the implant consisting of a reinforcing metallic core and composite laminates (mutually transversally connected layers of a composite – lamellas). In the composite layers, the modulus of elasticity is gradually changing in the radial direction, which means that it is decreasing in the direction towards a stem surface (or towards the interface of a live tissue). The modulus of elasticity of the last (surface) lamina is approximately identical to the modulus of elasticity of the *corticalis*. In the composite stem, the gradient of elastic properties is thus achieved. For the four laminas, the following expression applies:

$$y = 0.17 * x^{-1.1}$$

The effects of bending moments, torque moments, normal and shearing forces were verified on the finite-element-method models. The distributions of stress fields σ_y are shown in Fig. 1.

Conclusions: On the basis of the performed numerical analyses, the following most significant conclusions can be made:

1) The bending stress acting on the system of a femur *diaphysis* – a composite implant (with the gradient of elastic properties) leads to **the increase in the strain of the medial lamellas of the composite, and in the decrease in the strain of the surface lamella.** Its strain on the interface between the live tissue and the composite is identical to the strain of the bone tissue. The normal **compressive stresses** of $\sigma_y = -22.9$ MPa were verified in the 2nd and 3rd medial lamellas of the composite; the normal **tensile stresses** of $\sigma_y = 15$ MPa also in the 3rd and 2nd lateral lamellas of the composite (Fig. 1).
2) **The bending stresses increase the normal stresses σ_y in the medial lamellar layers** of the implant stem composite, and substantially **decrease these stresses in its surface lamella.**
3) The surface layers of the composite implant and the adjacent part of the medial wall of the *corticalis* (in the medullar canal) have the identical (without a sudden "leap") compressive stresses in bending (Fig. 1). It is evident that the selection of the gradient of elastic properties resulted in **achieving the identical compressive normal stress both in the live material and in the inanimate material.**
4) **The tensile stresses** of the surface layers of the composite implant and the adjacent layers of the lateral wall of the *corticalis* (in the proximity of the medullar canal) are **identical**. In these locations, the live tissue and the inanimate composite are identically stressed.

Acknowledgements: The presented paper has been supported by the GACR, grant No. 106/03/00255 and VZ No. 240000012.

References

[1] A. Jíra, *A Composite Biotolerant Hip Implant*, a Diploma Thesis, CVUT, Faculty of Civil Engineering, 2002.
[2] P. Malchau, P. Herberts and A. Söderman, *Odén: Prognosis of Total Hip Replacement*, Congress AAOS, USA
[3] J. Valenta et al., *Biomechanics, a monograph, Academia*, Prague 1985.

Materials to reconstruct complex defects of the skull and midface

E. Röpke and M. Bloching
MLU- Halle-Wittenberg, Department of Oto-Rhino-Laryngology HNS, Halle/Saale, Germany
Tel.: +49 0345 5522876; Fax: +49 0345 5522864; E-mail:ernst.roepke@medizin.uni-halle.de

Defect covering of the skull and midface is indicated by functional or cosmetic reasons. Materials used for such reconstructions are selected considering different criteria: 1) localisation, 2) size of the defect, 3) quality of covering, 4) insertion into chronically infected environment, 5) mechanical stability, 6) biocompatibility, 7) costs.

To differentiate between transplants or implants: transplants originate from living organism, implants consist of non-biological material.

Autogenous transplants are taken from the patient. The outer table of the calvarium, the tabula externa, is prefered for the reconstructions of the skull or the orbital region. Some advantages are the proximity to the defect, the high firmness and the low danger of resorption. One disadvantage is the bad mouldability.

Vital transplants are necessary for a transplantation into an area supplied with inadequate blood circulation. In such a case tabula externa petiolated at the m. temporalis is suitable.

Furthermore, microvascularly anastomosed bone-transplants from different donor areas can be taken. Defects of the back of frontal sinus, the skull base or the orbital floor can be supplied with autogenous cartilage by the cartilaginous septum, by the Cavum conchae or by the cartilaginous rib.

Defects of soft tissue are reconstructed with autogenous flaps, for example transplants of the m. temporalis or microvascularly anastomosed flaps like the free radial forearm flap.

Non-biological materials are called implants or alloplastics. The longest experiences with implants are collected with metals, particularly titanium. Titanium is used as prefabricated implants. These implants are exactly fitted to the defects preoperatively on the basis of computertomographic data. The biocompatibility of titanium is good, the implants are mechanically stable. Disadvantageous is the impossibility of an intraoperative adaptation, the weight, the high thermal conductivity and the high costs.

Synthetic implants used in medicine are very versatile. Porous polyethylene is well-proven in the surgery of head and neck. The biocompatibility is good. It is elastic and contrary to ceramics it is not brittle. Advantageous is the possibility to fit the implant intraoperatively and a relatively low price. But complications by inflammation are possible in case a free contact exists of the plastics to sinuses. Another synthetic implant is the polymethylmetacrylate. It is used frequently as cement. Mixed with two components, the implant can be produced intraoperatively and fitted to the defect within five minutes, but there is a problem with the strongly exothermic reaction during the polymerization. Bioactive ceramics have the advantage of an interaction with the surrounding vital tissue, especially with bones. Hydroxyapatite, a calcium phosphate, is used for reconstruction of the skull. Other bioactive ceramics are glass ceramics. As well as a good biocompatibility they can be fitted very well intraoperatively. In comparison to titanium the mechanical stability is not so strong.

The hydroxyapatite cement “BoneSource” is produced by adding water to a combination of calcium phosphate salts. The so produced mass can be adapted for about 20 minutes. It is offered to fill or cover small skull defects. The granulate “NovaBone” is more economical. Contacting living tissue the surface changes into layer of calcium phosphate.

If a transplantation or an implantation is not possible in difficult cases, an epiprosthetic supply can be carried out. The epiprostheses are today produced from high-quality materials and made by a skilled expert giving absolutely satisfactory results.

Growth of chondrocytes on modified polyethylene surfaces – Analysis of autologous bioimplants

I. Schön and E. Röpke
Department of Oto-Rhino-Laryngology HNS, MLU- Halle-Wittenberg, Halle/Saale Germany
Tel.: +49 0345 5522876; Fax: +49 0345 5522864; E-mail: ernst.roepke@medizin.uni-halle.de

Introduction: The *in vitro* engineering of human cartilage is of great interest in the field of reconstitutive surgery. For the reconstruction of larger areas it is helpful to support the native tissue by the use of non-resorbable matrices seeded with autologous chondrocytes to suppress the immune response and furthermore to accelerate the integration of the implant into the surrounding tissue. Several different materials were proposed but the optimal synthetic matrix has not yet been found.

We used MEDPOR®, a linear high density polyethylene with a pore size of about 35–250 μm established as a non-resorbable prosthetic replacement material. This is used in different fields of reconstitutive surgery with good results. The aim of our work is further to improve the integration of

this prosthetic non-resorbable implant material into the surrounding living tissue by means of tissue engineering principles. In order to improve the adhesion of the cells on the surface we used collagen II as biological glue between the synthetic matrix and the chondrocytes.

In former studies we examined the growth of chondrocytes on modified polyethylene surfaces. From these results we chose the sample modifications for this study.

The problem had been and is to find out which modification yields the best results in establishing a functional artificial cartilage construct and in which way one can distinguish between reimplanted cells and surrounding tissue.

Methods: In this study we used three different MEDPOR®-samples: MEDPOR®-without any modification, MEDPOR®- coated with collagen II and MEDPOR®-functionalized by oxygen plasma treatment, coupled with collagen II. The analytical experiments were performed with polyethylene samples 10 mm in diameter. For fluorescence labeling the cells grown at the MEDPOR®-samples were incubated with the fluorescent dye DilC_{18} Histological examination of the samples was performed after fixation in 2% paraformaldeyde-PBS.

Fixed samples were cut into 4 μm slices and the fluorescence labeled slices had been visualized by confocal laser scanning microscopy and fluorescence microscopy.

Results and discussion: The aim of our study was to describe tissue engineered hybrid systems of chondrocytes grown at modified polyethylene surfaces before and after implantation and to compare these with implants of unmodified polyethylene implants. Therefore, we analyzed the polyethylene samples before implantation.

The amount of collagen II, brought to the surface, was determined by ELISA. From these data one could conclude the oxygen plasma treatment lead to more bound collagen. The main question was, did more bound collagen led to more cells at the artificial modified surface. To answer this question we did the MTT-assay. The viability of the cells in dependency of the surface modification was compared. The effects of the surface modification had been smaller than expected. From the results of these experiments it seemed to be useful to do an oxygen plasma treatment in case of collagen coating. As already mentioned, without significant improvement of cell adherence

The labelling with the fluorescence marker DilC18 allowed to follow the integration of the *in vitro* grown chondrocytes into the surrounding tissue. In future experiments it is necessary to optimise these procedures. With MRI-technique we tried to follow the integration of the implant into the surrounding tissue. We received some images but they are not of good quality. Further images have to be taken to improve the representation.

Elastic, dielectric and piezoelectric coefficients of langasite-type crystals

U. Straube[a], H. Beige[b], J. Bohm[b], R.B. Heimann[a], T. Hauke[a] and M. Hengst[b]
[a]*Martin-Luther-Universität Halle-Wittenberg, Fachbereich Physik, Friedemann-Bach-Platz 6, 06108 Halle/Saale, Germany*
[b]*Technische Universität Bergakademie Freiberg, Institut für Mineralogie, 09596 Freiberg, Germany*
Fax: +49 345 55 27 604; E-mail: u.straube@physik.uni-halle.de

Introduction: Langasite-type crystals are promising new materials for ultrasound transducers.The investigated compounds lanthanum gallium silicate (langasite, LGS, $La_3Ga_5SiO_{14}$), lanthanum gallium niobate (langanite, LGN, $La_3Ga_{5.5}Nb_{0.5}O_{14}$), and lanthanum gallium tantalate (langataite, LGT,

$La_3Ga_{5.5}Ta_{0.5}O_{14}$) belong to the same trigonal acentric crystal class 32 like quartz. These crystals have rather high electromechanical coupling coefficients and are mechanical robust. They are suitable for the construction of transducers generating very pure longitudinal and transversal acoustical waves in a broad frequency and temperature region. All linear elastic, dielectric and piezoelectric coefficients of these crystals were determined at room temperature. The ultrasound pulse overlap technique was used to get sound velocities in different crystal directions for the determination of the elastic coefficient tensor. The piezoelectric properties were found with a quasistatic apparatus in comarison to quartz. The piezoelectric coefficients are about three times larger than those of quartz. The sound propagation in piezoelectric crystals is treated in [2] and in [3]. The elastic stiffness coefficients can be calculated using Christoffel's equation $(\lambda_{ik} - \rho v^2 \delta_{ik}) = 0$ with $\lambda_{ik} = c_{ijkl} n_j n_l + (e_{nij} n_n n_j e_{mkl} n_m n_l)/(\varepsilon_{mn} n_m n_l)$. The c_{ijkl} denote the elastic stiffness coefficients at constant electric field, u_k the particle displacements, ρ the density and δ_{ik} Kronecker's symbol. The direction cosines nm and nl are directed along the normal vector of the wave front. The piezoelectric stress coefficients e_{nij} and the dielectric coefficients ε_{mn} are necessary to include the sound velocity change due to the piezoelectricity. The abbreviated matrix notation (e.g. [3]) is used in the following text. The linear elastic behaviour for crystals with the symmetry 32 is described by six independent elastic coefficients $c_{11}, c_{12}, c_{13}, c_{14}, c_{33}$ and c_{44}. Two piezoelectric coefficients d11 and d14 and two dielectric coefficients ($\varepsilon_{11} = \varepsilon_{22}$, ε_{33}) were to be determined.

Experimental: All measurements were done at room temperature. Langasite-type materials have the same symmetry like quartz with a hexagonal cross section normal to the nonpolar axis, denoted by Z-axis. The axis between opposite corners is called X-axis. The remaining Y-axis joins opposite faces. Langasite-type crystals are grown from powdered high purity (99.99%) oxides using the Czochralski technique. The x-ray density was calculated using the lattice parameters: $\rho_{\mathrm{LGS}} = 5.754$ g/cm^3, $\rho_{\mathrm{LGN}} = 5.908$ g/cm^3, $\rho_{\mathrm{LGT}} = 6.151$ g/cm^3 [1]. The measurements of the piezoelectric coefficients were performed using parallelepipeds of approximately $10 \times 5 \times 5$ mm^3 size cut from the as-grown crystals in three different orientations:

(i) edges parallel to the crystallographic X-, Y-, Z-axes,
(ii) 45° rotated to the X-axis, and
(iii) rotated by 45[a] around the Y-axis.

The crystal samples were carefully ground to achieve parallel end faces and flat surfaces. An equipment based on a capacitive detector was used for measurements of the piezoelectric strain coefficients d_{mi} [4]. The piezoelectric coefficient d_{11} was found with electric field and dilatation directions along the x-direction. The absolute value of d_{14} could be estimated from a 45° rotated Y-sample. According to the IEEE standard [5], d_{11} is defined as having positive sign.

Dielectric measurements were performed using a General Radio 1621 Precision Capacitance Measurement System at a frequency of 800 Hz. X- and Y-cut quartz transducers of 20 MHz center frequency were bonded to the samples to generate longitudinal and transverse sound waves. The measurement of the sound velocity was carried out using the Papadakis method [6]. The measurements were carried out on samples oriented (i) with their edges parallel to the X, Y, Z-axes, and (ii) rotated by 45° around the X-axis.

Results: The measured piezoelectric strain coefficients and the dielectric coefficients are summarized in Table 1.

The selected sound velocities of Table 2 were used to calculate the elastic stiffness coefficients. The first sign in the square brackets of the longitudinal velocities v_l or the transversal velocities v_t denote the wave propagation direction, the second sign the (sometimes approximate) polarization direction, Z_d means degenerate.

Table 1
Piezoelectric strain coefficients d_{mi} and relative dielectric coefficients ε_{mn}

	LGS	LGN	LGT
d_{11} [10^{-12} m/V]	6.15	7.41	7.06
d_{14} [10^{-12} m/V]	−6.01	−6.61	−4.32
ε_{11}	19.2	20.7	19.6
ε_{33}	50.7	79.0	76.5

Table 2
Selected phase velocities of LGS, LGN and LGT, see text for further explanation

	LGS	LGN	LGT
Longitudinal velocities [m/s]			
v_l [X/X]	5770	5683	5567
v_l [Z/Z]	6780	6632	6560
Transverse velocities [m/s]			
v_t [Z_d]	3076	2902	2888
v_t [X/Y]	2386	2290	2258
v_t [X/Z]	3321	3175	3133
v_t [$-45°$/X]	2444	2332	2303
v_t [$-45°$/45°]	3410	3237	3178

Table 3
Piezoelectric stress coefficients and elastic stiffness coefficients for LGS, LGN and LGT

	LGS	LGN	LGT
Piezoelectric stress coefficients			
e_{11} [C/m^2]	0.43	0.518	0.510
e_{14} [C/m^2]	−0.145	−0.099	−0.025
Elastic stiffness coefficients			
c_{11} [G/Pa]	189.82	189.25	188.94
c_{12} [G/Pa]	106.57	107.71	108.13
c_{13} [G/Pa]	97.54	99.36	100.86
c_{14} [G/Pa]	14.73	14.00	13.91
c_{33} [G/Pa]	263.54	259.72	264.44
c_{44} [G/Pa]	54.24	49.73	51.25

The connection of the piezoelectric stress coefficients e_{11} and e_{14} to the piezoelectric strain coefficients is shown in the following formulas:

$$e_{11} = d_{11}(c_{11} - c_{12}) + d_{14}c_{14},$$
$$e_{14} = 2d_{11}c_{14} + d_{14}c_{44}.$$

The system of equations of elastic coefficients, piezoelectric coefficients and dielectric coefficients is implicit and was solved using MATHEMATICA. The result of this calculation is summarized in Table 3 showing piezoelectric stress coefficients and elastic stiffness coefficients.

Acknowledgements: The authors thank Dr. Dubiel, Martin-Luther-University Halle for the experimental support concerning the dielectric measurements and Drs. V. Alex and B. Lux, Institute of Crystal Growth Berlin for preparing the samples. The support by the DFG is acknowledged.

References

[1] J. Bohm, R.B. Heimann, M. Hengst, R. Roewer and J. Schindler, *J. Crystal Growth* **204** (1999), 128.
[2] V.E. Ljamov, *Polarization Effects and the Anisotropy of Acoustic Wave Interaction in Crystals*, in Russian, University Press, Moscow, 1983.
[3] T. Ikeda, *Fundamentals of Piezoelectricity*, Oxford Science Publications, Oxford, 1990.
[4] G. Sorge, T. Hauke and M. Klee, *Ferroelectrics* **163** (1995), 77.
[5] IEEE Standard on Piezoelectricity, ANSI/IEEE Std 176-1987, New York, 1988.
[6] E.P. Papadakis, *J. Acoustic Soc. Am.* **42** (1967), 1045.
[7] J. Bohm, E. Chilla, C. Flannery, H.-J. Fröhlich, T. Hauke, R.B. Heimann, M. Hengst and U. Straube, *J. Crystal Groth* **216** (2000), 293.
[8] E. Chilla, C. Flannery, H.-J. Fröhlich, J. Bohm, R.B. Heimann, M. Hengst and U. Straube, *Proceeedings of the IEEE Ultrasonics Symposium* (2002), 377–380.